Dendrochronologia 86 (2024) 126238

Contents lists available at ScienceDirect

Dendrochronologia

journal homepage: www.elsevier.com/locate/dendro

A multi-centennial drought reconstruction from tree-rings reveals a growing threat to Christmas Island's water resources

S. Sharifazari [a,*], J.G. Palmer [b,c,d], F. Johnson [a], C.S.M. Turney [b,c,d,e], M.S. Andersen [f]

[a] Water Research Centre, School of Civil and Environmental Engineering, University of New South Wales, Australia
[b] ARC Centre of Excellence in Australian Biodiversity and Heritage, University of New South Wales, Australia
[c] Chronos 14Carbon-Cycle Facility, Mark Wainwright Analytical Centre, University of New South Wales, Australia
[d] Earth and Sustainability Science Research Centre, School of Biological, Earth and Environmental Sciences, University of New South Wales, NSW 2515, Australia
[e] Division of Research, University of Technology Sydney, Ultimo, New South Wales, Australia
[f] Water Research Laboratory, School of Civil and Environmental Engineering, University of New South Wales, Australia

ARTICLE INFO

Keywords:
Climate variability
Dendrochronology
Indian Ocean
ScPDSI
Small islands
Water supply

ABSTRACT

Small islands that depend on limited freshwater resources are at significant risk from seasonal drought, which poses a major threat to both their ecosystems and communities. Christmas Island, located in the eastern Indian Ocean, presents an example for which severe drought conditions during the wet season not only affects its freshwater resources but also biodiversity on the island, including the migration pattern of the iconic red crab species. However, short-term instrumental climate records on this island make it hard to quantify drought variability and assess its associated risks. Tree growth is affected by drought via reduced soil moisture, and hydroclimate reconstruction from tree-ring chronologies can therefore provide longer-term information on historical variability of dry and wet periods. Here, we reconstructed the wet season (December-May) self-calibrating Palmer Drought Severity Index (scPDSI) for Christmas Island using 64 remote tree-ring chronologies from Asia, Australia, and New Zealand. scPDSI was reconstructed using the Point-to-Point Regression (PPR) method and compared with regional marine coral proxies for independent verification. The remote tree-ring chronologies explained more than 66 percent of scPDSI variance (R-squared) over the calibration period. The trees identified as significant predictors in the regression model were primarily located in areas affected by the Indo-Pacific climate drivers including the Indian Ocean Dipole (IOD). The reconstructions span 1540 CE to 2000. During the first four centuries of this period, the frequency of extreme (5th percentile) droughts and pluvial events rarely exceeded one event per 13 years. In contrast, the frequency of both extremes experienced an unprecedented increase during the 20th century, and with a notable shift towards dry conditions. These findings highlight a significant shift towards more frequent and severe dry conditions during the wet season on Christmas Island, posing a challenge to water resource management and potentially threatening the island's ecosystem and services to the community.

1. Introduction

Christmas Island, located in the eastern part of the Indian Ocean, is an isolated island renowned for its abundant tropical rainforests and remarkable biodiversity (Misso and West, 2014). It provides habitat for numerous endangered migratory and endemic species, including seabirds and land crabs. Like many other small oceanic islands, it is particularly vulnerable to the impacts of climate change, with threats to its biodiversity and freshwater availability (Maunsell Australia, 2009). Regional climate change projections are for reduced precipitation and increasing periods of drought for Christmas Island by the end of the century (Maunsell Australia, 2009). However, considerable uncertainties remain around the future projections. In addition, the limited number and duration of instrumental hydroclimate records makes it challenging to accurately quantify the magnitude of natural climate variability. This limits the context for future projected changes of Christmas Island, which is impacted by multiple climatic drivers.

Christmas Island lies at the southern edge of the intertropical convergence zone (ITCZ) and the north-western edge of the Australian summer monsoon domain. This results in a tropical monsoonal climate

* Corresponding author.
E-mail address: s.sharifazari@unsw.edu.au (S. Sharifazari).

https://doi.org/10.1016/j.dendro.2024.126238
Received 8 August 2023; Received in revised form 19 June 2024; Accepted 9 July 2024
Available online 14 July 2024

with distinct wet and dry seasons based on the Köppen-Geiger climate classification (Beck et al., 2018). It shares the same type of climate with most parts of Java, Indonesia, which is the closest landmass to Christmas Island (~350 km), characterised by a wet season typically starting in November/December and ending in April/May when the north-west monsoon winds prevail (Ferijal et al., 2021; Hutchings and Brown, 2014). Both the El Niño–Southern Oscillation (ENSO) and the Indian Ocean Dipole (IOD) cause inter-annual variations of the monsoon onset in the region, however, they appear to have negligible impact on the total monsoon precipitation (Hamada et al., 2012; Zhang and Moise, 2016). Although the majority of the Australian summer monsoon domain has shown an upward trend in precipitation since 1950, a decrease in summer precipitation has been observed in some parts of the northwestern region of the domain, i.e., south Sumatra and Java Islands, in close proximity to Christmas Island (Aldrian and Djamil, 2008; Zhang and Moise, 2016). These areas have also experienced an increase in the severity of drought during the wet season demonstrated by an increasing trend in the number of observed dry spells (Ferijal et al., 2021).

The regional drying trend for the wet season combined with the observed declining trend for spring precipitation in Christmas Island (Maunsell Australia, 2009) has increased the risk of severe dry episodes on the island. Such dry conditions threaten hydrological drought through reduced soil moisture and reduced rainfall recharge into its underground karstic water supply source, with wider impacts on ecosystem services. For instance, delays to the start of the rainy season may force the iconic red crabs, which play a crucial role in preserving the structure and species composition of the rainforest vegetation on Christmas Island (Hutchings and Brown, 2014), to change their migration pattern (Shaw and Kelly, 2013). Unlike other natural hazards, drought is a 'creeping disaster', and it is difficult to identify when it starts or ends (Kiem et al., 2016). This challenge is intensified for Christmas Island with a lack of long-term hydroclimate data, impeding our understanding of the range of its natural hydroclimate variability.

Paleoclimate data, specifically annually-resolved tree-ring chronologies, can provide additional information on the range of natural hydroclimate variability (Meko and Woodhouse, 2011). Annual tree-ring widths (i.e., tree growth) and drought share common climatic controlling factors such as soil moisture deficit, precipitation, and temperature (D'Arrigo and Smerdon, 2008; Palmer et al., 2015). Thus, tree-ring-derived records can be valuable proxies (i.e., predictors) for extending instrumental climate-derived drought indices back in time. Although some tree species on Christmas Island such as *Terminalia catappa* may have dendrochronological potential (Castor Neto et al., 2023), there is currently no established tree-ring proxy available for Christmas Island. Two different coral proxies have been developed for the island. However only one proxy is publically available and it only covers a short period of 24 years within the instrumental period, making it unsuitable for the purpose of this study (Marshall and McCulloch, 2001). The longer coral proxy, i.e., 118 years, is not publicly available, and other attempts to develop a speleothem proxy have been unsuccessful (Hargreaves et al., 2023; Hua et al., 2012). Although local proxies can detect climate patterns at a local scale, as well as regional and longer-term scales, using remote proxies for paleoclimate reconstruction has been proven to be successful in the absence of local proxies (Higgins et al., 2023; Higgins et al., 2022). Given that the climate of Christmas Island is predominantly shaped by the large-scale Indo-Pacific climate drivers, tree-ring sites from the broader region with similar climate drivers (Allen et al., 2020; Cook et al., 2010; Palmer et al., 2015) could potentially be employed for drought reconstruction on the island. Such a reconstruction would provide long-term baseline data to assess drought variability and allow comparison to climate model projections. Thus, it might assist in identifying climate models that better capture historical climate extremes (e.g., droughts) on Christmas Island, leading to more informative future projections. The lack of accurate future projections has been recognized as one of the primary gaps in the last assessment report of the Intergovernmental Panel on Climate Change (IPCC) for small island states (SIDS; Mycoo et al., 2022).

Here we develop a reconstruction of the self-calibrating Palmer Drought Severity Index (scPDSI) spanning several centuries to aid in understanding drought variability during the December to May rainy season in Christmas Island. The scPDSI index for the target season is reconstructed from a network of remote tree-ring proxies using the reliable Point-to-Point Regression (PPR) technique (Cook et al., 2010). We assess the consistency of our reconstruction with other paleoclimate archives by comparing it to marine coral proxies from adjoining regions. We then explore the pattern of drought variability, the occurrence of megadroughts (Cook et al., 2022), and the changes in the frequency of extreme events over the last five centuries and their relationship with the Indo-Pacific climate forcings. Finally, we discuss how our methodology can help extend baseline data and reduce the uncertainty in future climate projections for small oceanic islands.

2. Study area and Data

2.1. Study area

Christmas Island is an uplifted, composite, reef carbonate island (Grimes, 2001) located in the north-eastern part of the Indian Ocean, approximately 350 km south of Java and 2600 km northwest of Perth, Australia (Fig. 1). The island covers an area of roughly 135 square kilometres, and Murray Hill is the highest point of the island, with an elevation of 361 m above sea level. Christmas Island has a tropical monsoonal climate with an average precipitation of about 2200 mm/year. Rainforest covers most parts of the island, and due to its outstanding biodiversity and high conservation values, 63 % of the island has been classified as National Park (Hutchings and Brown, 2014). It has a karst drainage system, so almost all precipitation goes quickly underground through this system without forming any surface watercourses (Barrett, 2001). The karstic landscape provides a water supply source for local households and businesses on Christmas Island through a set of seasonally recharged cave streams and springs (Barrett, 2001; West et al., 2020).

2.2. Climate data

Temperature and precipitation have been recorded at several weather stations on the island. Although precipitation data starts from June 1901, around 60 % of precipitation records are missing for the period between 1940 and 1960. The records of air temperature on the island start from January 1921. However, the corresponding gauge-based Climate Research Unit (CRU) temperature field for Christmas Island provides monthly temperature series for the island back to 1900. The CRU data and the corresponding gauge observations match well over their overlapping period. Given this similarity and the small range of temperature variation in the tropics, we used the corresponding CRU TSv4.05 (Harris et al., 2021) temperature field series to calculate the scPDSI for Christmas Island. We also used the CRU scPDSI field for global land (Barichivich et al., 2022) and the Hadley Centre Sea Surface Temperature (HadlSST; Rayner et al., 2003) data set for our spatial correlation analyses. Supplementary Table S1 summarizes the climate features of Christmas Island. The target season for our drought reconstruction is the wet season (December to May), which accounts for more than 70 % of the total annual precipitation on the island.

2.3. Tree-ring data

For this study, we identified publicly available tree-ring records located in areas known to be affected by Indo-Pacific climate drivers in previously published drought atlases, primarily from the Monsoon Asia Drought Atlas (MADA) but also the eastern Australia and New Zealand summer drought atlas (ANZDA) and a few from the European Russia Drought Atlas (Allen et al., 2020; Cook et al., 2010; Cook et al., 2020;

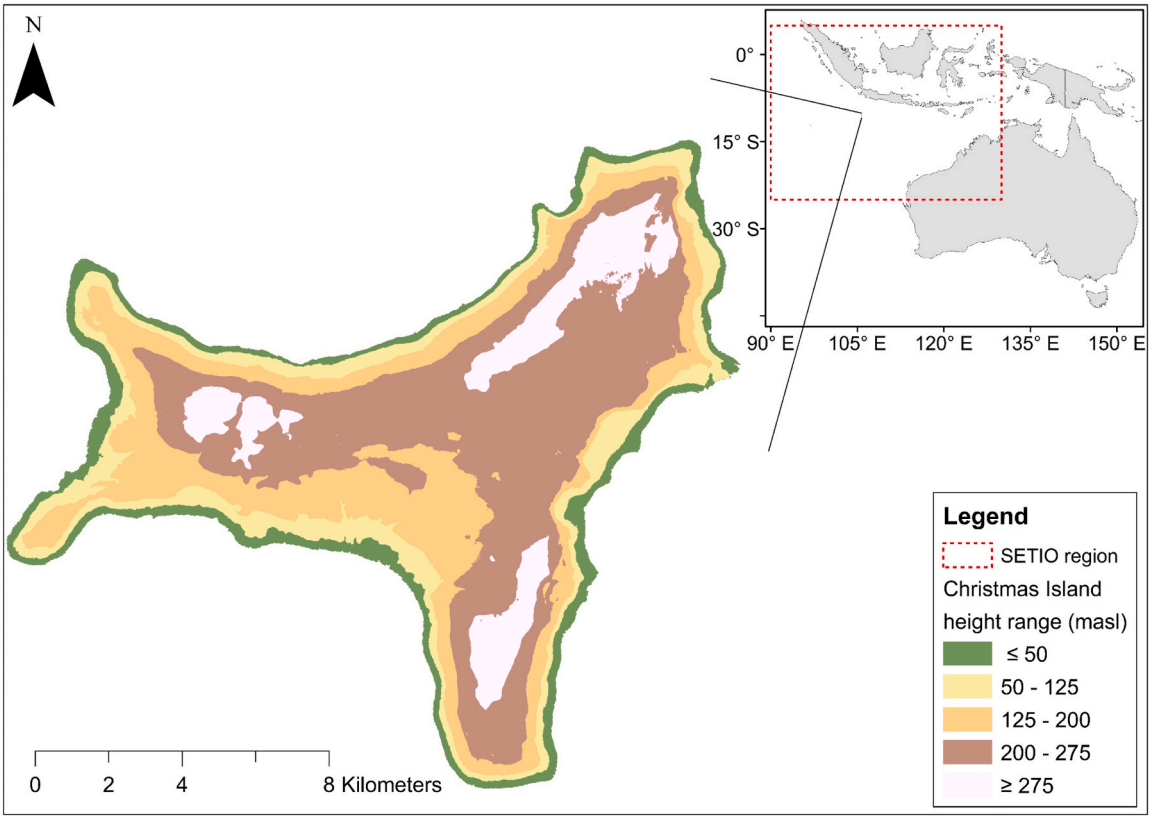

Fig. 1. Topography of the Christmas Island and its geographic location with regard to Australia and the south-eastern tropical Indian Ocean (SETIO; Du et al., 2005) region.

Palmer et al., 2015). The available records include an initial pool of approximately 800 annual tree-ring series scattered over a vast area, including east Türkiye, Asia south of 50°N, Australia, and New Zealand. The raw tree-ring records were all standardized following the same method as described by Cook et al. (2020) and used by O'Donnell et al. (2021). The first step involved applying adaptive power transformations to the raw ring-width measurements to ensure they were more homoscedatic and calculating the ring-width indices as residuals (Cook and Peters, 1997). The next stage involved using an age-dependent spline (Melvin et al., 2007) to remove low-frequency variance thought to be mainly due to non-climatic age/size-related changes in ring width over time. This was followed by 'signal-free' detrending (Melvin and Briffa, 2008) aimed at helping to minimise trend distortion and improve the resolution of medium-frequency variance from the series of tree-ring measurements. All of the above standardisation steps were done using the 'RCSsigfree' program (https://www.geog.cam.ac.uk/research/projects/dendrosoftware/ developed by Ed Cook, Paul Krusic, Kenneth Peters and Tom Melvin in 2017). The chronologies obtained from this process were then used as initial predictors for our drought reconstruction model.

3. Methods

3.1. Instrumental drought

Drought indices are quantitative measures for drought characterization. To be consistent with previous studies on drought reconstruction, we chose scPDSI as the drought index in this study (Wells et al., 2004). scPDSI is a commonly used drought index, which calculates the deviation of soil moisture from its climatological average using a simple water balance model. Its calculation requires monthly precipitation and temperature, as well as parameters representing the soil water holding capacity. As the available CRU gridded product for this index does not cover Christmas Island, we used the scPDSI R package developed by Zhong et al. (2019) to calculate the index for Christmas Island. The package requires monthly precipitation, potential evapotranspiration (PET), and soil water-holding capacity to calculate scPDSI. Given the limited availability of meteorological data for Christmas Island, monthly potential evapotranspiration was computed using Thornthwaite's method (McMahon et al., 2013) through the MATLAB tool developed by Jacobi et al. (2013). The Thornthwaite method, while valuable for estimating PET in data-limited areas such as Christmas Island due to its simplicity, only accounts for temperature dependencies of atmospheric evaporative demand (Trenberth et al., 2014). This dependence on temperature can lead to overestimates of PET, particularly after 1980 when temperatures increased significantly at a global rate of 0.28 °C per decade (Cook et al., 2014; Osborn et al., 2021). Consequently, it has been found that using Thornthwaite PET in scPDSI calculations can lead to more severe estimates of recent droughts compared to the use of PET derived from the Penman-Montieth method (Sheffield et al., 2012). Thus, the modest temperature increase of only 0.4 °C on Christmas Island from 1974 to 2008 (Maunsell Australia, 2009) may slightly overestimate recent droughts, especially in these analyses where the post-2000 instrumental data has been appended to the reconstruction. The soil parameters were obtained from Australian soil resource information system database (https://www.asris.csiro.au/) for scPDSI calculation. We then averaged the six monthly scPDSI values from the prior year (t-1) December through the current year (t) May as the current year wet season scPDSI for the predictand in our regression model.

3.2. Reconstruction model

Consistent with previous drought reconstructions (Cook et al., 2010; Cook et al., 2007; Palmer et al., 2015), we used the nested point-to-point

principal component regression (PPR) method in this study. PPR retains the tree-ring chronologies that significantly correlate ($p \leq 0.1$; Spearman, Pearson, and robust Pearson) with the scPDSI during a common calibration period. The retained chronologies are then categorized into successive groups of chronologies (nests), with the first nest including all retained chronologies and representing the shortest time span as determined by the youngest chronology. The next younger chronologies are then sequentially dropped from the chronology pool when going further back in time (Meko, 1997). No further nest is formed when there are less than two chronologies remaining. For each nest, the regression model is applied on the principal components (PCs) of tree-ring chronologies from that nest, i.e., regression model predictors for that nest, during the calibration period. Tree-ring PCs are entered in the stepwise regression by order of explanatory variance, determined by Akaike Information Criterion (AIC) criterion in our case. The variance of the reconstruction obtained from each nest is scaled to that of the instrumental data over the calibration period. Finally, the model appends the reconstruction of longer nests to the start year of the younger ones to develop the final reconstruction.

To build the PPR model, we only used chronologies that extended up to and beyond 2000 CE, i.e., chronologies with the end year of greater than or equal to 2000. The end date of scPDSI reconstruction (2000) was chosen as a trade-off between a declining pool of chronologies and maximising the length of the overlapping instrumental period for calibrating the regression model. Since ~60 % of precipitation records were missing for the period between 1940 and 1960, we excluded this period from the analysis. Thus, the most reliable instrumental data of the period after 1961 were used for model calibration and the period of 1903–1940 was withheld to verify the model. In addition to unlagged chronologies, we included the one-year lagged tree chronologies (i.e., t+1) to be retained in the chronology pool, as the previous year's climate condition may affect tree growth of the current year (Rao et al., 2018). To account for large-scale, remote teleconnections, a large search radius, i.e., 10,000 kilometres, was set to identify chronologies that are significantly correlated with scPDSI. However, the sensitivity of the results to a smaller search radius was also investigated by building the regression model on trees located closer than 3000 kilometres from Christmas Island. We also used the first order autoregressive (AR) prewhitening technique to reduce non-climate effects. The application of AR prewhitening assists in resolving large differences in short-term autocorrelation between climate and tree rings, which are caused by the influence of physiological and stand dynamics on annual ring widths (Cook et al., 1999).

To estimate the PPR model uncertainty, we used the maximum entropy bootstrapping (MEBoot) method (Vinod, 2006; Vinod and Lopez-de-Lacalle, 2009). MEBoot is a random perturbation method that applies to both the tree-ring and scPDSI series, preserving the overall stochastic properties of the original time series used in the regression model (Cook et al., 2013). In so doing, it provides a suite of pseudo-reconstructions, i.e., 300 in our case, from which an empirical probability distribution function for each reconstructed year can be derived. The empirical probability distribution function can then be used to estimate the uncertainty of the reconstruction (Rao et al., 2018).

3.3. Model verification

The reconstruction was validated by evaluating the overall performance statistics as well as comparing the reconstruction to independent paleoclimate proxy records. The calibration period coefficient of multiple determination (CRSQ), the verification period reduction of error (VRE), and the verification period coefficient of efficiency (VCE) (Cook et al., 1999) were used to assess the performance of our reconstructions. VRE evaluates the reconstruction relative to the calibration mean and ranges from -∞ to 1, where values greater than zero indicate the superiority of the reconstructions over the calibration mean. VCE is equivalent to the Nash-Sutcliffe Coefficient of Efficiency in hydrology (Nguyen et al., 2020), and it is more rigorous than VRE as it measures the performance of reconstructions relative to the verification mean, always resulting in a smaller value compared to VRE unless the calibration and verification means are identical (Cook et al., 2010). The VRE and VCE are calculated as:

$$VRE = 1 - [\frac{\sum (y - \widehat{y}_i)^2}{\sum (y_i - \overline{y}_c)^2}]$$

$$VCE = 1 - [\frac{\sum (y_i - \widehat{y}_i)^2}{\sum (y_i - \overline{y}_v)^2}]$$

Where y_i and $\widehat{y}_i$ are observed and reconstructed scPDSI, respectively, $\overline{y}_c$ is the mean of the actual data in the calibration period, and $\overline{y}_v$ stands for the mean of the actual data in the verification period.

To verify the reconstruction against independent marine climate proxies (i.e., coral records), we first investigated the spatial footprint of sea surface temperature (SST) on the wet season scPDSI over the instrumental period of 1961–2000. We reduced our investigation to the areas located within 2500 km from Christmas Island, known to be the scale of the regional weather systems (Boers et al., 2019). This area covers most of the south-eastern tropical Indian Ocean region shown in Fig. 1. As the strongest positive relationship was found between the averaged June through November SST of the previous year and wet season scPDSI through our spatial correlation analyses (Fig. 2b), we used the average of the coral records over the corresponding months, i.e., June to November, for the independent verification.

3.4. Extreme event analysis

Extreme dry events were classified as those values located below the lower 5th percentile of the reconstruction mean. Similarly, extreme pluvial events were above the 95th percentile. The frequency of occurrence of these extreme events and how their frequency changes through the time is important for risk analysis (Mudelsee, 2020). However, the intervals between consecutive extreme dry events or consecutive extreme pluvial events are not normally distributed. Following Mudelsee et al. (2004), a non-parametric Gaussian kernel function was used to estimate the changes in the occurrence rates of extreme events. We used the 30-year bandwidth Gaussian kernel function and obtained a 90 % confidence band of the occurrence rates using 1000 bootstrap simulations.

Besides extreme dry and pluvial events, megadroughts lasting several years can have substantial impacts on the present-day communities, ecology, and ecosystem services (Cook et al., 2016). However, the process of defining megadroughts is complex due to the variety of methods used to determine their start and end dates, whether they are droughts or megadroughts (Coats et al., 2013; Cook et al., 2022; Meehl and Hu, 2006). This can result in different characteristics being attributed to megadrought events when considering a single reconstruction. To account for this methodological diversity and following Cook et al. (2022), we identified the extended drought periods with a minimum length of 5 years and explored the exceptional ones (i.e., megadroughts) in terms of severity and duration.

4. Results

4.1. Selected tree ring predictors and coral proxies

The screening criteria used by PPR retained 64 separate tree-ring chronologies, i.e., excluding the lagged versions, as the final predictors for scPDSI reconstruction based on the 10,000 km search radius. The selected trees are scattered over a vast area with the closest ones located in the Australian monsoon region, and including chronologies from Java just ~600 km from Christmas Island. Fig. 2a shows the locations of selected trees with regard to the geographic position of

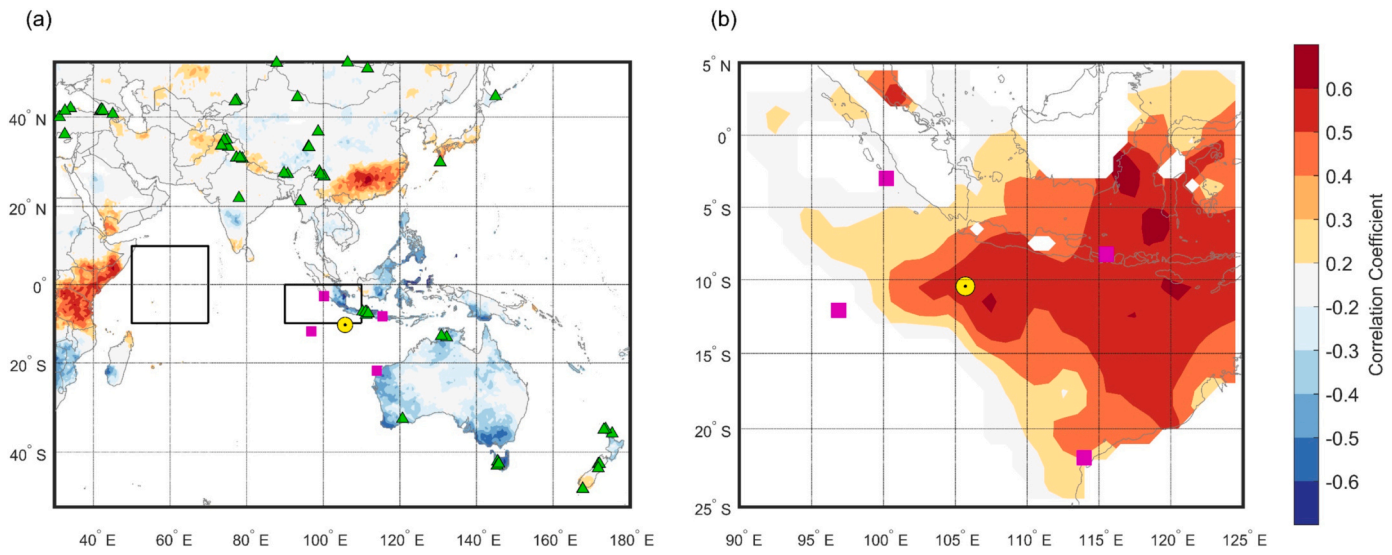

Fig. 2. (a) The locations of 64 tree-ring chronologies (green triangles) along with coral proxies (pink squares) and Christmas Island (yellow circle) plotted on the Pearson correlations (colour scale) between averaged June-November dipole mode index (differences in SST anomalies between western and eastern poles; black boxes) and December-May CRU scPDSI fields for the period of 1961–2000. (b) Significant Pearson correlations ($p<0.1$) between prior year (t-1) June-November HadlSST SST data and December-May scPDSI for the same period calculated using KNMI (Koninklijk Nederlands Meteorologisch Instituut) Climate Explorer (Trouet and Van Oldenborgh, 2013).

Christmas Island, IOD regions (Saji et al., 1999), and the location of coral proxies used for comparison in this study. Detailed information about the selected tree-ring chronologies and coral records are included in supplementary Table S2 and Table 1.

The underlying map in Fig. 2a shows the Pearson correlation between the June through November dipole mode index (DMI; Saji et al., 1999), i.e., the period of peak IOD activity, and December-May CRU scPDSI fields. Most of the selected trees are located in the MADA domain, where droughts were found to be associated with positive IOD events, especially when co-occurring with El Niño (Ummenhofer et al., 2013). The extent of the area affected by IOD stretches to the eastern Mediterranean, as suggested by tree-ring-based winter-to-spring temperature reconstruction from Türkiye (Heinrich et al., 2013). To further investigate the spatial configuration of the selected tree-ring chronologies for the final PPR model, the loadings of individual chronologies across space was evaluated. Figure S1 shows that both regional, i.e., trees located closer than 3000 kilometers distance to Christmas Island, and remote ones equally contributed to the reconstruction as indicated by the strength of their (absolute) correlations in the regression model.

Fig. 2b shows the significant Pearson correlations between the December-May scPDSI and SST data from the HadlSST data set (grid box 90–120°E, 5–25°S). Among different seasons, the prior year (t-1) June-November SST of the region had the highest positive correlation with scPDSI over the entire instrumental period, i.e., 1903–2019, with the strongest correlation for the most reliable period of 1961–2000. This high-correlated SST season corresponds to the seasons of peak IOD activity.

Out of the four monthly/bimonthly coral proxies within the box (Fig. 2b) indicated in Fig. 2(b), the proxy from Bali, Indonesia is in the region with the strongest SST-scPDSI correlation. The Bali coral provides information on the evolution of the Indian Ocean Dipole structure and its relationship with monsoonal variability (Charles et al., 2003). Thus, this coral proxy is as an independent paleo record to test the validity of our reconstruction for the period before our calibration window, i.e., before 1961. We also investigated the correlation of our reconstruction with other coral proxy records located in the south-eastern tropical Indian Ocean which are geographically close to Christmas Island but lie outside the monsoonal region. Some of these corals were recognized to be influenced by ENSO and IOD (Hennekam et al., 2018; Kuhnert et al., 2000), and they might therefore not entirely capture the climate drivers that affect our scPDSI reconstruction for Christmas Island.

Table 1
Pearson correlation comparing December-May scPDSI reconstruction with prior year (t-1) June-November coral $\delta^{18}O$ and Dipole Mode Index.

	Calibration period (1961–2000)			before 1960		
	n	r	p-value	n	r	p-value
Cocos (Keelings) Islands coral $\delta^{18}O$ (1809–2009)	40	-0.265	0.0986	151	0.077	0.3435
Southern Mentawai coral $\delta^{18}O$ (1936–2001)	40	-0.363	0.0214	23	-0.516	0.0118
Padang Bai (Bali) coral $\delta^{18}O$ (1782–1990)	30	-0.653	0.0001	177	-0.319	0
Ningaloo Reef coral $\delta^{18}O$ (1879–1994)	35	-0.328	0.0544	80	-0.239	0.0326
Coral-based DMI reconstruction (1846–2018)	40	-0.406	0.0094	113	-0.258	0.0055

4.2. Drought reconstructions

The final reconstruction for the averaged December-May scPDSI index for Christmas Island extends back to 1540 CE. The 64 tree-ring predictors explained more than ~66 % of the scPDSI variability over the calibration period of 1961–2000. Even the nest with the earliest start date (i.e., longest time span), with only 25 tree-ring predictors, explains more than 40 % of the scPDSI variability. Fig. 3 shows the median skill scores of the PPR model for the entire period of scPDSI reconstruction.

The positive VRE and VCE values for the entire period (i.e., the 5th percentiles of VCE and VRE are greater than zero) indicate meaningful information provided by reconstructions to help with drought interpretation over the last five centuries in Christmas Island. Although, the median reconstruction skill was positive for the period before 1540 back to 1400, we truncated our reconstruction at 1540, as the 5th percentile VCE was less than 0 before that time. The number of chronologies used for reconstruction is more than ~50 for most of the reconstruction and it starts to decrease from 1700 CE backward. However, the minimum number of predictors is 25, which is much higher than the minimum

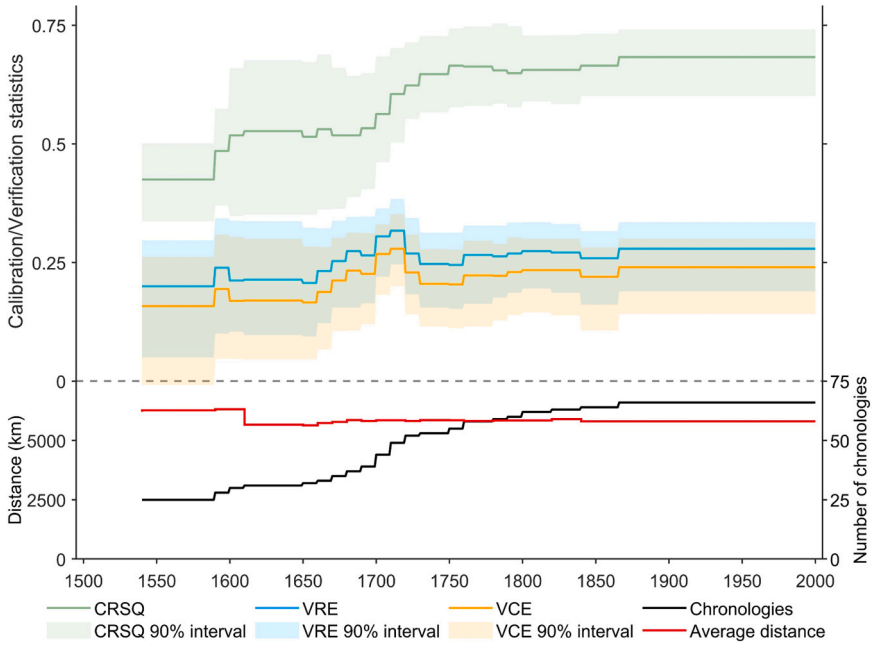

Fig. 3. Median reconstruction skills of the PPR model for each nest with the 90 % MEBoot confidence intervals (shaded areas). The bottom panel shows the number of tree-ring chronologies used for reconstruction in each nest and the average distance of the selected tree ring chronologies to Christmas Island.

required number, i.e., two chronologies, to form a nest in the nested approach.

Table 1 shows Pearson correlations comparing December-May scPDSI reconstruction and prior year (t-1) June-November coral $\delta^{18}O$ for the calibration (1961–2000) and pre-calibration (before 1960) periods. We also included the coral-based July-December DMI reconstruction (Abram et al., 2020) in our comparison. Consistent with the positive SST-scPDSI correlation (Fig. 2b), all coral proxies and the coral-based DMI reconstruction are negatively correlated with scPDSI ($p<0.1$) during the calibration period, with the strongest correlation for the coral proxy from Bali. The negative correlation applies for the period before 1960 except for Cocos (Keelings) Islands coral proxy, which is

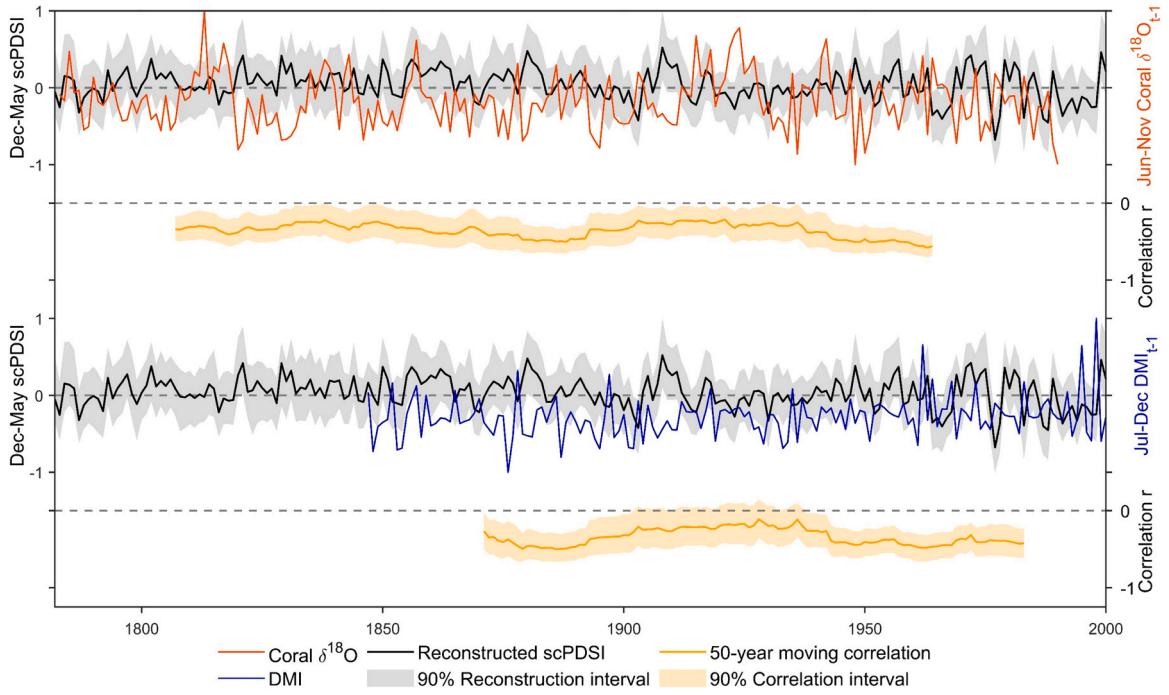

Fig. 4. Comparison of the reconstructed December-May scPDSI (black line) with prior year (t-1) June-November coral $\delta^{18}O$ records from Bali (red line) and prior year (t-1) July-December coral-based DMI reconstruction (blue line). The shaded grey area shows the 90 % confidence interval for scPDSI reconstructions; All values were scaled between −1 and 1 for a better visualization. The 50-year running correlations for December-May scPDSI vs. prior year (t-1) June-November coral $\delta^{18}O$ and December-May scPDSI vs. prior year (t-1) June-November reconstructed DMI shown in orange lines with the shaded orange area showing their 90 % confidence intervals based on 1000 bootstrap simulations. To remove the non-climate trend all series were detrended using the first-year difference method for correlation analyses.

located outside of the monsoonal region. Similar results are obtained using the Spearman rank correlation (table S3). Adjusting DMI reconstructions from Mentawai fossil corals within the corals dating uncertainty bounds (±13 years; Abram et al., 2020) gives the same negative DMI-scPDSI reconstruction for the different segments within the period of 1540–1820 (Table S4).

The 50-year moving correlations demonstrate that all significant relationships (Table 1) are stable for their corresponding overlapping periods based on the 90 % confidence interval of 50-year moving correlation. Fig. 4 shows the temporal stability of the Bali coral – scPDSI and the coral-based DMI – scPDSI relationship over the last two centuries and the results for other coral records are shown in Figure S2. Both prior year June-November coral $\delta^{18}O$ and prior year July-December coral-based DMI inversely follow our reconstructed December-May scPDSI.

We tested the sensitivity of our results to the search radius by repeating the analyses with a smaller search radius of 3000 kilometres. Table S5 compares the performance statistics of the reconstruction derived from these chronologies to the one for 10,000 kilometres. The results show that restricting the regression model to a smaller search radius does not dramatically change the performance of the model compared to the baseline reconstruction and the two reconstructions positively correlate over their overlapping period of 1700–2000 (Figure S3). Comparison against coral proxies also shows the validity of the regression model with a search radius of 3000 kilometers (Table S6). To further investigate the validity of the baseline reconstruction we compared it with the proxy-data assimilation product (PHYDA; Steiger et al., 2018) which provides a more physically-driven approach for scPDSI reconstruction. Although this product dose not completely cover our reconstruction in space or time, the December-February PHYDA reconstruction averaged over the grid points close to Christmas Island (box 105–115°E, 5–15°S) significantly correlate with our reconstruction over the entire reconstruction period (Pearson r = 0.17, p = 0.0003) providing additional evidence for the teleconnections between Christmas Island the selected tree-ring locations (Figure S4). It should be noted that the spatial correlation between the baseline reconstruction and PHYDA is a direct correlation rather than the negative correlation presented in Fig. 2a.

Fig. 5a shows the final reconstruction with its 90 % confidence interval compared with the instrumental period scPDSI index for the period after 1961. The reconstruction matches the instrumental scPDSI, capturing both interannual variability and extreme dry and wet events. The full reconstruction and its 90 % confidence interval are shown in Fig. 5b. As can be seen from this figure, dry events tended to be dominant compared to wet ones over the last five centuries, except perhaps during the nineteenth century. This pattern is deduced from the number of times the scPDSI value exceeded dry and wet thresholds (±0.99; Wells et al., 2004) shown by dashed lines. Recognized positive IOD events over the instrumental period, e.g., 1961, 1994, and 1997 correspond with dry December-May season in their subsequent years for both instrumental and reconstructed scPDSI series during the calibration period.

Using the methodology described in Section 3.4, we identified 16 extended drought periods throughout the entire reconstruction interval (Fig. 6). These droughts were longer for the pre-instrumental period with the longest one lasting for 14 years (1664–1677), compared to the drought experienced during 1990–1998. However, the severity of extended droughts during the instrumental period are unprecedented over the whole reconstruction interval. The lowest mean scPDSI of −2.2 was for the 1964–1968 drought, and −1.56 for the 1990–1998 drought compared to the most severe pre-instrumental droughts, i.e., 1605–1609 with a mean scPDSI of −1.62. Like the instrumental period, most of the severe positive IOD events identified by the coral-based DMI reconstruction (Abram et al., 2020) were followed by negative scPDSI values in the subsequent year (e.g., scPDSI < −1 for 1584 and 1660 events; Fig. 6).

4.3. Recurrence intervals of extremes

Fig. 7 shows the occurrence rate curves of extreme drought and pluvial events with their estimated 90 % confidence intervals. Extreme drought events were identified as the years for which their corresponding December-May scPDSI values were below the 5th percentile of reconstructions, shown in vertical orange lines in the top of Fig. 7 (with the opposite case for high extreme wet events indicated with green lines). The return period of both extreme drought and pluvial events was relatively large before 1900, with the minimum of ~13 years for extreme pluvial and drought events in ~1860 and ~1600, respectively. From the late 16th century to late 18th century extreme pluvial events were generally less frequent than their corresponding drought events. Since 1900, there has been an increasing trend in the occurrence rate of

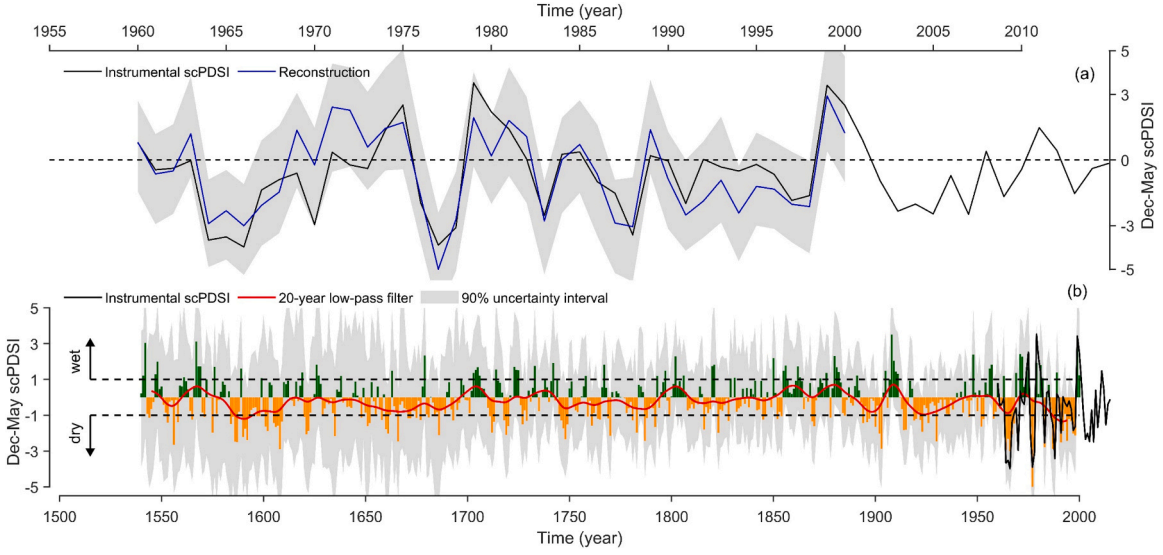

Fig. 5. (a) Instrumental (black) versus reconstructed (blue) averaged December-May scPDSI for Christmas Island over the instrumental period 1961–2015. (b) Reconstructed averaged December-May scPDSI with the 90 % confidence interval for reconstruction shown in grey. Reconstruction values greater than zero are shown in vertical dark green lines and values less than zero are shown in dark orange. The solid red line shows the 20-year low-pass filtered reconstruction and the horizontal dashed black lines indicate dry and wet thresholds.

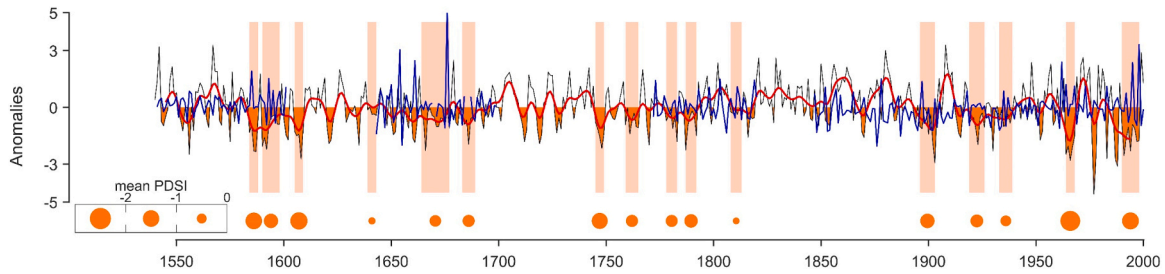

Fig. 6. Reconstructed averaged December-May scPDSI (black line) with the 10-year low-pass filter (red line) and prior year (t-1) July-December coral-based DMI reconstruction (blue line). The light orange bars represent the extended droughts with their mean scPDSI shown in orange circles.

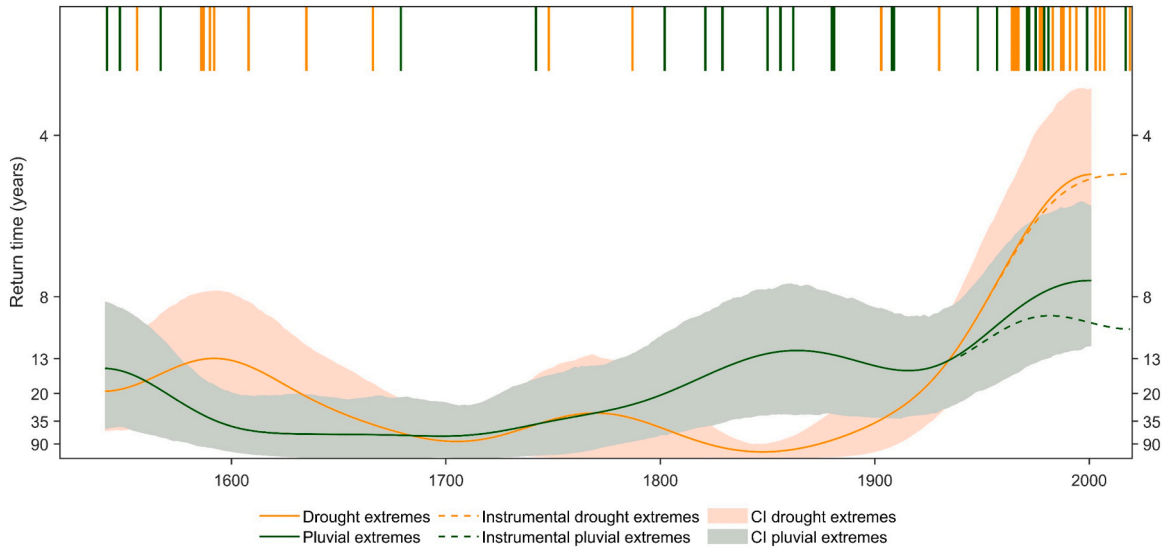

Fig. 7. Extreme droughts and pluvials December-May and the time-varying frequency of the occurrence of these events between 1540 and 2000, with dashed lines showing the adjusted frequency curve if instrumental data is appended to the reconstruction after 2000. A kernel occurrence rate estimator (Mudelsee et al., 2003, Silva et al., 2012) was used with a bandwidth of 30 years (solid lines). The shaded areas (green and orange) represent the 90 % confidence intervals based on 1000 bootstrap simulations.

both extremes, and reaching the unprecedented return time of ~4 years for dry events and ~8 years for wet events by the end of the 20th century. During the 20th century, extreme droughts were more frequent than extreme wet events. Appending the observations to the reconstructions and extending the end date of reconstruction from 2000 to 2019 makes this difference even more obvious (i.e., return times of ~4.5 years compared to 10 years; see dashed lines in Fig. 7), indicating a continuing trend towards drier conditions.

5. Discussion

Both modelling skill metrics and comparison against coral $\delta^{18}O$ proxy records and the coral-based DMI reconstruction verify the reliability of our reconstruction. Most of tree-ring chronologies retained in our reconstruction were recognized to be informative on the Indo-Pacific climate drivers such as IOD and ENSO in previous regional studies (Allen et al., 2020; D'Arrigo et al., 2006) and drought atlases (Cook et al., 2010; Palmer et al., 2015). These drivers strongly affect the interannual climate variability on Christmas Island as evidenced by hydroclimate observations and the strontium/calcium (Sr/Ca) ratios of a short, modern local coral proxy (Marshall and McCulloch, 2001). Developing more local climate proxies and incorporating them into the predictor pool of the reconstruction model would enhance the ability of the reconstruction model to better capture the full spectrum of climate variability, especially at a local-scale. However, local coral proxies recently developed from Christmas Island showed a strong relationship with salinity variations caused by the strength of the Indonesian throughflow rather than local precipitation (Hargreaves et al., 2023). A similar relationship was suggested for coral proxies from Cocos (Keeling) Islands (Hennekam et al., 2018), which may help explain the instability in its correlation to our scPDSI reconstruction. The successful development of regional tree-ring chronologies from African tropical rainforests suggests that similar tree species on Christmas Island could potentially be used to develop local chronologies (De Ridder et al., 2013).

The negative relationship between DMI and our December-May scPDSI reconstruction shows the significant impacts of the IOD on drought variability in Christmas Island during the wet season. Parts of the wet season's scPDSI variability is related to its prior June-November dry season, i.e., the seasonal phase lock of the IOD cycle, due to the inherent memory in the scPDSI of previous climate conditions. However, IOD is highly correlated to the September-November (SON) precipitation in the eastern tropical Indian Ocean and a positive IOD event is often accompanied by strong easterly anomalies, which weaken the monsoon westerlies, cause precipitation decreases, and delay the wet season onset (Kurniadi et al., 2021; Zhang and Moise, 2016). Even though the IOD typically weakens after the SON season, its effects still persist during December-January and contribute to interannual monsoon variability in conjunction with ENSO (Zhang and Moise, 2016).

Proxy evidence has widely confirmed that the 17th century witnessed a notable extreme variability in the tropical Indo-Pacific

associated with the high variability in IOD and ENSO (Abram et al., 2020; Freund et al., 2019). Our scPDSI reconstruction shows a high occurrence rate of extreme dry events and several extended droughts during the 17th century with the 1664–1677 drought being the longest drought over the last five centuries (Fig. 6). The 17th century also marked the driest mean conditions experienced by both the Asian and Australian summer monsoons throughout the past thousand years (Denniston et al., 2016; Yan et al., 2015). The extended dry periods that occurred in the late 17th century are consistent with the fossil coral records found in southern Mentawai, which indicate a high variability of positive Indian Ocean Dipole (IOD) events during this period (Abram et al., 2020). However, during the 20th century, the occurrence rate of both extremes has substantially increased, with the return time reducing to ~4 for dry and ~8 years for wet extremes by the end of the reconstruction. Since the mid-twentieth century, there has been a rise in the frequency of concurrent El Niño and positive phase of Indian Ocean Dipole events, which contribute to dry conditions in the region (Xiao et al., 2022). The more frequent occurrence of positive IOD events during this time period has been accompanied by an intensification of their magnitude (Abram et al., 2008).

Small islands are highly exposed to the dynamic impacts of severe droughts. For example, the El Niño-related 2015–2016 drought in Vanuatu, resulted in a significant reduction of their freshwater sources (Iese et al., 2021). Instrumental records of hydroclimate variables may provide some useful information about drought variability of these islands (Herrera and Ault, 2017; McGree et al., 2016). However, the available hydroclimate observations are too short to capture the full range of natural climate variability, and climate models selected solely based on these records produce highly uncertain future projections (Schmidt et al., 2013). The most recent IPCC report indicates a lack of clear patterns in observed changes in precipitation and drought, and low confidence in their projected changes for most Small Island Developing States (SIDS; Mycoo et al., 2022). In the absence of high-resolution local paleoclimate data, proxies from regions with strong teleconnections can provide valuable long-term baseline data for these islands, helping to quantify the range of natural climate variability and constrain climate models. Selecting an ensemble of climate models based on their ability to match both historical records and paleoclimate reconstructions for these islands can address the structural uncertainty in future projections (Schmidt et al., 2013). This could involve using the paleo component of the climate models to hindcast hydroclimate variables over pre-instrumental period, e.g., the Last Millennium (LM; 850–1850 CE), and then comparing them to the reconstructed records from tree-ring proxies in both time and frequency domains (Lovejoy and Schertzer, 2012; Schmidt et al., 2013). In our case, the modelled scPDSI can be calculated from simulated temperature and precipitation series by climate models and then evaluated against the reconstructed scPDSI from climate proxies.

The drying trend, combined with human caused factors such as the introduction of invasive species (Baumgartner II and Ryan, 2020; Shaw and Kelly, 2013), increases the risks to the survival of Christmas Island's red crab population. Additionally, this trend could have an impact on the community of the island by reducing the seasonal recharge into its karstic water supply source. Considerable seasonal and interannual variation in discharge flows have been estimated for springs and cave streams on Christmas Island with a lagged response of one to five months to rainfall for the peak flow (Grimes, 2001; West et al., 2020). Severe dry conditions during the December-May wet season adversely affect the amount of water storage in the epikarst above the aquifer at the start of the wet season of the subsequent year (Grimes, 2001), leading to reduced or even insufficient water supply if the dry condition persists over multiple years. Thus, as experienced in other small oceanic islands (Moglia et al., 2008; Mycoo, 2007; Payet and Agricole, 2006; White et al., 2007), economic and management failures in the water sector could potentially happen during extended droughts on Christmas Island.

6. Conclusions

In this study, we used a suite of remote tree-ring proxies from regions with strong teleconnections to develop the first December-May wet season scPDSI reconstruction for Christmas Island. The reconstruction skill, together with its independent verification against marine coral proxies from nearby regions, showed that it contains useful information about drought variability over the last five centuries in the island. Thus, it helps in overcoming challenges associated with drought characterization posed by the limited availability of long-term hydroclimate records.

Our reconstruction indicates that extreme dry and wet events occurred with nearly equal frequency during the period 1540–1900, but there was a higher occurrence of extended drought conditions. However, the frequency of both extremes experienced an unprecedented increase during the 20th century, with a notable bias towards dry conditions. The finding highlights a significant shift towards more frequent and severe dry conditions during the wet season on Christmas Island. Given the vulnerability of key endemic species of the island (e.g., the red crab), and its water supply system to dry conditions, this shift may negatively impact the biodiversity of the island (Hutchings and Brown, 2014; Shaw and Kelly, 2013) and reduce its freshwater availability by decreasing the discharge rate of springs and cave streams. When combined with previous research on the influential climate drivers in the area, such as the Indian Ocean Dipole (IOD), this work raises concerns about the future resilience of the island's community and ecosystem services during these transformations and provide planners and water resource managers with information to plan appropriately for sustainable future developments and their associated water use requirements.

Declaration of Competing Interest

The authors declare that they have no known competing financial interests or personal relationships that could have appeared to influence the work reported in this paper.

Data availability

Data will be made available on request.

Acknowledgments

The authors acknowledge the efforts of all the dendrochronologists who have contributed tree-ring chronologies to the ITRDB, allowing for studies such as this one to be undertaken. Our thanks to the editor and anonymous reviewers, whose comments have improved this manuscript. SSH is supported by Australian Government Research Training Scholarships and the UNSW Scientia PhD Scholarship Schemes. FJ is supported by the UNSW Scientia Program and the Australian Research Council Training Centre in Data Analytics for Resources and Environments. The University of New South Wales facilitated open access publishing as part of the Wiley - University of New South Wales agreement via the Council of Australian University Librarians.

Appendix A. Supporting information

Supplementary data associated with this article can be found in the online version at doi:10.1016/j.dendro.2024.126238.

References

Abram, N.J., et al., 2020. Coupling of Indo-Pacific climate variability over the last millennium. Nature 579 (7799), 385–392. https://doi.org/10.1038/s41586-020-2084-4.

Abram, N.J., Gagan, M.K., Cole, J.E., Hantoro, W.S., Mudelsee, M., 2008. Recent intensification of tropical climate variability in the Indian Ocean. Nat. Geosci. 1 (12), 849–853. https://doi.org/10.1038/ngeo357.

Aldrian, E., Djamil, Y.S., 2008. Spatio-temporal climatic change of rainfall in East Java Indonesia. Int. J. Climatol. 28 (4), 435–448 https://doi.org/10.1002/joc.1543.
Allen, K.J., et al., 2020. Hydroclimate extremes in a north Australian drought reconstruction asymmetrically linked with Central Pacific Sea surface temperatures. Glob. Planet. Change 195, 103329. https://doi.org/10.1016/j.gloplacha.2020.103329.
Maunsell Australia, 2009. Climate change risk assessment for the Australian Indian Ocean Territories, Commonwealth Attorney-General's Department. Canberra: Australia.
Barichivich, J., Osborn, T.J., Harris, I., van der Schrier, G., Jones, P., 2022. Monitoring global drought using the self-calibrating Palmer Drought Severity Index.
Barrett, P.J., 2001. Searching for water on Christmas Island. Helictite 37 (2), 37–39.
Baumgartner II, N.R., Ryan, S.D., 2020. Interaction of red crabs with yellow crazy ants during migration on Christmas Island. Math. Biosci. 330, 108486.
Beck, H.E., et al., 2018. Present and future Köppen-Geiger climate classification maps at 1-km resolution. Sci. Data 5 (1), 180214. https://doi.org/10.1038/sdata.2018.214.
Boers, N., et al., 2019. Complex networks reveal global pattern of extreme-rainfall teleconnections. Nature 566 (7744), 373–377. https://doi.org/10.1038/s41586-018-0872-x.
Castor Neto, T.C., Penetra Cerveira Lousada, J.L., Fontana, C., Gomes Moreira, C., Vicente de Figueiredo Latorraca, J., 2023. The Influence of Rainfall and Temperature on Radial Growth of Urban Trees Under the Impact of Steel Industry Pollution. BioResources 18 (3).
Charles, C.D., Cobb, K., Moore, M.D., Fairbanks, R.G., 2003. Monsoon–tropical ocean interaction in a network of coral records spanning the 20th century. Mar. Geol. 201 (1), 207–222 https://doi.org/10.1016/S0025-3227(03)00217-2.
Coats, S., Smerdon, J.E., Seager, R., Cook, B.I., González-Rouco, J.F., 2013. Megadroughts in southwestern North America in ECHO-G millennial simulations and their comparison to proxy drought reconstructions. J. Clim. 26 (19), 7635–7649.
Cook, E.R., et al., 2010. Asian Monsoon Failure and Megadrought During the Last Millennium. Science 328 (5977), 486–489. https://doi.org/10.1126/science.1185188.
Cook, E.R., et al., 2013. Five centuries of Upper Indus River flow from tree rings. J. Hydrol. 486, 365–375. https://doi.org/10.1016/j.jhydrol.2013.02.004.
Cook, B.I., et al., 2016. North American megadroughts in the Common Era: reconstructions and simulations. WIREs Clim. Change 7 (3), 411–432. https://doi.org/10.1002/wcc.394.
Cook, E.R., et al., 2020. The European Russia Drought Atlas (1400–2016 CE. Clim. Dyn. 54 (3), 2317–2335. https://doi.org/10.1007/s00382-019-05115-2.
Cook, B.I., et al., 2022. Megadroughts in the Common Era and the Anthropocene. Nat. Rev. Earth Environ. 3 (11), 741–757. https://doi.org/10.1038/s43017-022-00329-1.
Cook, E.R., Meko, D.M., Stahle, D.W., Cleaveland, M.K., 1999. Drought Reconstructions for the Continental United States*. J. Clim. 12 (4), 1145–1162. https://doi.org/10.1175/1520-0442(1999)012<1145:Drftcu>2.0.Co;2.
Cook, E.R., Peters, K., 1997. Calculating unbiased tree-ring indices for the study of climatic and environmental change. Holocene 7 (3), 361–370. https://doi.org/10.1177/095968369700700314.
Cook, E.R., Seager, R., Cane, M.A., Stahle, D.W., 2007. North American drought: Reconstructions, causes, and consequences. Earth-Sci. Rev. 81 (1), 93–134. https://doi.org/10.1016/j.earscirev.2006.12.002.
Cook, B.I., Smerdon, J.E., Seager, R., Coats, S., 2014. Global warming and 21st century drying. Clim. Dyn. 43 (9), 2607–2627. https://doi.org/10.1007/s00382-014-2075-y.
D'Arrigo, R., et al., 2006. Monsoon drought over Java, Indonesia, during the past two centuries. Geophys. Res. Lett. 33 (4) https://doi.org/10.1029/2005GL025465.
D'Arrigo, R., Smerdon, J.E., 2008. Tropical climate influences on drought variability over Java, Indonesia. Geophys. Res. Lett. 35 (5) https://doi.org/10.1029/2007GL032589.
De Ridder, M., et al., 2013. A tree-ring based comparison of Terminalia superba climate–growth relationships in West and Central Africa. Trees 27 (5), 1225–1238. https://doi.org/10.1007/s00468-013-0871-3.
Denniston, R.F., et al., 2016. Expansion and contraction of the Indo-Pacific tropical rain belt over the last three millennia. Sci. Rep. 6 (1), 34485.
Du, Y., Qu, T., Meyers, G., Masumoto, Y., Sasaki, H., 2005. Seasonal heat budget in the mixed layer of the southeastern tropical Indian Ocean in a high-resolution ocean general circulation model. J. Geophys. Res.: Oceans 110 (C4). https://doi.org/10.1029/2004JC002845.
Ferijal, T., Batelaan, O., Shanafield, M., 2021. Rainy season drought severity trend analysis of the Indonesian maritime continent. Int. J. Climatol. 41 (S1), E2194–E2210. https://doi.org/10.1002/joc.6840.
Freund, M.B., et al., 2019. Higher frequency of Central Pacific El Niño events in recent decades relative to past centuries. Nat. Geosci. 12 (6), 450–455. https://doi.org/10.1038/s41561-019-0353-3.
Grimes, K.G., 2001. Karst features of Christmas Island (Indian Ocean). Helictite 37 (2), 41–58.
Hamada, J.-I., et al., 2012. Interannual rainfall variability over northwestern Jawa and its relation to the Indian Ocean Dipole and El Niño-Southern Oscillation events. Sola 8, 69–72.
Hargreaves, J.A., Abram, N., Mallela, J., 2023. 118-year hydroclimate reconstruction from Christmas Island (Indian Ocean); an extended record of variability in the Indonesian Throughflow. Copernic. Meet.
Harris, I.C., Jones, P., Osborn, T., 2021. CRU TS4.05: Climatic Research Unit (CRU) Time-Series (TS) version 4.05 of high-resolution gridded data of month-by-month variation in climate (Jan. 1901- Dec. 2020). Centre for Environmental Data Analysis.
Heinrich, I., Touchan, R., Dorado Liñán, I., Vos, H., Helle, G., 2013. Winter-to-spring temperature dynamics in Turkey derived from tree rings since AD 1125. Clim. Dyn. 41 (7), 1685–1701. https://doi.org/10.1007/s00382-013-1702-3.
Hennekam, R., et al., 2018. Cocos (Keeling) Corals Reveal 200 Years of Multidecadal Modulation of Southeast Indian Ocean Hydrology by Indonesian Throughflow. Paleoceanogr. Paleoclimatology 33 (1), 48–60. https://doi.org/10.1002/2017PA003181.
Herrera, D., Ault, T., 2017. Insights from a New High-Resolution Drought Atlas for the Caribbean Spanning 1950–2016. J. Clim. 30 (19), 7801–7825. https://doi.org/10.1175/JCLI-D-16-0838.1.
Higgins, P.A., et al., 2022. Unprecedented High Northern Australian Streamflow Linked to an Intensification of the Indo-Australian Monsoon. e2021WR030881 Water Resour. Res. 58 (3). https://doi.org/10.1029/2021WR030881.
Higgins, P.A., Palmer, J.G., Andersen, M.S., Turney, C.S.M., Johnson, F., 2023. Extreme events in the multi-proxy South Pacific drought atlas. Clim. Change 176 (8), 105. https://doi.org/10.1007/s10584-023-03585-2.
Hua, Q., et al., 2012. Robust chronological reconstruction for young speleothems using radiocarbon. Quat. Geochronol. 14, 67–80. https://doi.org/10.1016/j.quageo.2012.04.017.
Hutchings, E., Brown, D., 2014. Christmas Island National Park Management. Plan 2014–2024.
Iese, V., et al., 2021. Historical and future drought impacts in the Pacific islands and atolls. Clim. Change 166 (1), 19. https://doi.org/10.1007/s10584-021-03112-1.
Jacobi, J., Perrone, D., Duncan, L.L., Hornberger, G., 2013. A tool for calculating the Palmer drought indices. Water Resour. Res. 49 (9), 6086–6089. https://doi.org/10.1002/wrcr.20342.
Kiem, A.S., et al., 2016. Natural hazards in Australia: droughts. Clim. Change 139 (1), 37–54. https://doi.org/10.1007/s10584-016-1798-7.
Kuhnert, H., Pätzold, J., Wyrwoll, K.H., Wefer, G., 2000. Monitoring climate variability over the past 116 years in coral oxygen isotopes from Ningaloo Reef, Western Australia. Int. J. Earth Sci. 88 (4), 725–732. https://doi.org/10.1007/s005310050300.
Kurniadi, A., Weller, E., Min, S.-K., Seong, M.-G., 2021. Independent ENSO and IOD impacts on rainfall extremes over Indonesia. Int. J. Climatol. 41 (6), 3640–3656. https://doi.org/10.1002/joc.7040.
Lovejoy, S., Schertzer, D., 2012. Stochastic and scaling climate sensitivities: Solar, volcanic and orbital forcings. Geophys. Res. Lett. 39 (11) https://doi.org/10.1029/2012GL051871.
Marshall, J.F., McCulloch, M.T., 2001. Evidence of El Niño and the Indian Ocean dipole from Sr/Ca derived SSTs for modern corals at Christmas Island, eastern Indian Ocean. Geophys. Res. Lett. 28 (18), 3453–3456. https://doi.org/10.1029/2001GL012978.
McGree, S., Schreider, S., Kuleshov, Y., 2016. Trends and Variability in Droughts in the Pacific Islands and Northeast Australia. J. Clim. 29 (23), 8377–8397. https://doi.org/10.1175/JCLI-D-16-0332.1.
McMahon, T.A., Peel, M.C., Lowe, L., Srikanthan, R., McVicar, T.R., 2013. Estimating actual, potential, reference crop and pan evaporation using standard meteorological data: a pragmatic synthesis. Hydrol. Earth Syst. Sci. 17 (4), 1331–1363. https://doi.org/10.5194/hess-17-1331-2013.
Meehl, G.A., Hu, A., 2006. Megadroughts in the Indian Monsoon Region and Southwest North America and a Mechanism for Associated Multidecadal Pacific Sea Surface Temperature Anomalies. J. Clim. 19 (9), 1605–1623. https://doi.org/10.1175/JCLI3675.1.
Meko, D., 1997. Dendroclimatic reconstruction with time varying predictor subsets of tree indices. J. Clim. 10 (4), 687–696.
Meko, D.M., Woodhouse, C.A., 2011. Application of streamflow reconstruction to water resources management. Dendroclimatology. Springe 231–261.
Melvin, T.M., Briffa, K.R., Nicolussi, K., Grabner, M., 2007. Time-varying-response smoothing. Dendrochronologia 25 (1), 65–69. https://doi.org/10.1016/j.dendro.2007.01.004.
Melvin, T.M., Briffa, K.R., 2008. A "signal-free" approach to dendroclimatic standardisation. Dendrochronologia 26 (2), 71–86. https://doi.org/10.1016/j.dendro.2007.12.001.
Misso, M., West, J., 2014. Conservation management of the terrestrial biodiversity of Christmas Island: challenges and perspectives. Raffles Bulletin of Zoology.
Moglia, M., Perez, P., Burn, S., 2008. Water troubles in a Pacific atoll town. Water Policy 10 (6), 613–637.
Mudelsee, M., 2020. Statistical Analysis of Climate Extremes. Cambridge University Press, Cambridge, pp. 68–102. https://doi.org/10.1017/9781139519441.006.
Mudelsee, M., Börngen, M., Tetzlaff, G., Grünewald, U., 2004. Extreme floods in central Europe over the past 500 years: Role of cyclone pathway "Zugstrasse Vb". J. Geophys. Res.: Atmospheres 109 (D23). https://doi.org/10.1029/2004JD005034.
Mycoo, M., 2007. Diagnosis of Trinidad's water problems (mid-1980s to mid-1990s). Water Policy 9 (1), 73–86.
Mycoo, M. et al., 2022. Small Islands. In: Climate Change 2022: Impacts, Adaptation, and Vulnerability. Contribution of Working Group II to the Sixth Assessment Report of the Intergovernmental Panel on Climate Change [H.-O. Pörtner, D.C. Roberts, M. Tignor, E.S. Poloczanska, K. Mintenbeck, A. Alegría, M. Craig, S. Langsdorf, S. Löschke, V. Möller, A. Okem, B. Rama (eds.)], Cambridge University Press, Cambridge, UK and New York, NY, USA, pp. 2043-2121. DOI:10.1017/9781009325844.017.
Nguyen, H.T.T., Turner, S.W.D., Buckley, B.M., Galelli, S., 2020. Coherent Streamflow Variability in Monsoon Asia Over the Past Eight Centuries—Links to Oceanic Drivers. e2020WR027883 Water Resour. Res. 56 (12). https://doi.org/10.1029/2020WR027883.
O'Donnell, A.J., McCaw, W.L., Cook, E.R., Grierson, P.F., 2021. Megadroughts and pluvials in southwest Australia: 1350–2017 CE. Clim. Dyn. 57 (7), 1817–1831. https://doi.org/10.1007/s00382-021-05782-0.

Osborn, T.J., et al., 2021. Land Surface Air Temperature Variations Across the Globe Updated to 2019: The CRUTEM5 Data Set. e2019JD032352 J. Geophys. Res.: Atmospheres 126 (2). https://doi.org/10.1029/2019JD032352.
Palmer, J.G., et al., 2015. Drought variability in the eastern Australia and New Zealand summer drought atlas (ANZDA, CE 1500–2012) modulated by the Interdecadal Pacific Oscillation. Environ. Res. Lett. 10 (12), 124002 https://doi.org/10.1088/1748-9326/10/12/124002.
Payet, R., Agricole, W., 2006. Climate change in the Seychelles: implications for water and coral reefs. AMBIO: A J. Hum. Environ. 35 (4), 182–189.
Rao, M.P., et al., 2018. Six Centuries of Upper Indus Basin Streamflow Variability and Its Climatic Drivers. Water Resour. Res. 54 (8), 5687–5701. https://doi.org/10.1029/2018WR023080.
Rayner, N., et al., 2003. Global analyses of sea surface temperature, sea ice, and night marine air temperature since the late nineteenth century. J. Geophys. Res.: Atmospheres 108 (D14).
Saji, N.H., Goswami, B.N., Vinayachandran, P.N., Yamagata, T., 1999. A dipole mode in the tropical Indian Ocean. Nature 401 (6751), 360–363. https://doi.org/10.1038/43854.
Schmidt, G.A., et al., 2013. Using paleo-climate comparisons to constrain future projections in CMIP5. Clim. Discuss. 9 (1), 775–835. https://doi.org/10.5194/cpd-9-775-2013.
Shaw, A.K., Kelly, K.A., 2013. Linking El Niño, local rainfall, and migration timing in a tropical migratory species. Glob. Change Biol. 19 (11), 3283–3290. https://doi.org/10.1111/gcb.12311.
Sheffield, J., Wood, E.F., Roderick, M.L., 2012. Little change in global drought over the past 60 years. Nature 491 (7424), 435–438. https://doi.org/10.1038/nature11575.
Steiger, N.J., Smerdon, J.E., Cook, E.R., Cook, B.I., 2018. A reconstruction of global hydroclimate and dynamical variables over the Common Era. Sci. Data 5 (1), 180086. https://doi.org/10.1038/sdata.2018.86.
Trenberth, K.E., et al., 2014. Global warming and changes in drought. Nat. Clim. Change 4 (1), 17–22. https://doi.org/10.1038/nclimate2067.
Trouet, V., Van Oldenborgh, G.J., 2013. KNMI Climate Explorer: a web-based research tool for high-resolution paleoclimatology. Tree-Ring Res. 69 (1), 3–13.
Ummenhofer, C.C., D'Arrigo, R.D., Anchukaitis, K.J., Buckley, B.M., Cook, E.R., 2013. Links between Indo-Pacific climate variability and drought in the Monsoon Asia Drought Atlas. Clim. Dyn. 40 (5), 1319–1334. https://doi.org/10.1007/s00382-012-1458-1.
Vinod, H.D., 2006. Maximum entropy ensembles for time series inference in economics. J. Asian Econ. 17 (6), 955–978. https://doi.org/10.1016/j.asieco.2006.09.001.
Vinod, H.D., Lopez-de-Lacalle, J., 2009. Maximum Entropy Bootstrap for Time Series: The meboot R Package. J. Stat. Softw. 29 (5), 1–19. https://doi.org/10.18637/jss.v029.i05.
Wells, N., Goddard, S., Hayes, M.J., 2004. A self-calibrating Palmer drought severity index. J. Clim. 17 (12), 2335–2351.
West, K.M., et al., 2020. Under the karst: detecting hidden subterranean assemblages using eDNA metabarcoding in the caves of Christmas Island, Australia. Sci. Rep. 10 (1), 21479. https://doi.org/10.1038/s41598-020-78525-6.
White, I., et al., 2007. Challenges in freshwater management in low coral atolls. J. Clean. Prod. 15 (16), 1522–1528.
Xiao, H.-M., Lo, M.-H., Yu, J.-Y., 2022. The increased frequency of combined El Niño and positive IOD events since 1965s and its impacts on maritime continent hydroclimates. Sci. Rep. 12 (1), 7532. https://doi.org/10.1038/s41598-022-11663-1.
Yan, H., et al., 2015. Dynamics of the intertropical convergence zone over the western Pacific during the Little Ice Age. Nat. Geosci. 8 (4), 315–320.
Zhang, H., Moise, A., 2016. The Australian summer monsoon in current and future climate. The Monsoons and Climate Change. Springer, pp. 67–120.
Zhong, Z., He, B., Guo, L., Zhang, Y., 2019. Performance of Various Forms of the Palmer Drought Severity Index in China from 1961 to 2013. J. Hydrometeorol. 20 (9), 1867–1885. https://doi.org/10.1175/JHM-D-18-0247.1.